ISET Journal of Earthquake Technology, Paper No. 409, Vol. 38, No.1, March 2001, pp. 17-29

SITE-SPECIFIC GROUND MOTION PREDICTION USING 3-D MODELLING

J.P. Narayan
Department of Earthquake Engineering
University of Roorkee, Roorkee-247667

ABSTRACT

An algorithm was developed for the simulation of 3-D elastodynamic wave propagation using displacement-stress relations. The parsimonious staggered grid scheme was adopted instead of the standard staggered grid scheme since it requires less computational memory. The double-couple point shear dislocation source was implemented into the numerical grid by using the moment tensor components as the body force couples. Anelastic attenuation was incorporated in the modelling by applying a simple attenuation function. Simulations of a half-space model for different grid sizes using a fixed amount of moment per unit volume are in accordance with the effective total moment used. Snapshots of a layered model reveal the accuracy and stability of the scheme at different discontinuities. The effect of soil velocity on amplitude amplification and increase in signal duration was studied and results depict increase in amplification and duration with decrease of velocity in the surficial layer. Further, it was found that horizontal components were more amplified as compared to the vertical component.

KEYWORDS: 3-D Modelling, Moment Tensor Source Formulation, Radiation Pattern and Attenuation

INTRODUCTION

The site-specific strong ground motion (SGM) prediction depends very much on the radiation pattern and the local site conditions. So, the SGM prediction, taking into account the energy released, 3-D radiation pattern, path effect and local site conditions, is of prime importance in earthquake engineering. The study of effects of local site conditions on the characteristics of the SGM has been and continues to be a field of active research, since high-frequency SGM is the least understood area due to the lack of ground motion records. The recent researches in this area include the works of Anderson et al. (1986), Mikumo and Miyatake (1987), Vidale and Helmberger (1987), Frankel and Vidale (1992), Olsen et al. (1995), Boore and Joyner (1997), and Narayan (2000). In the past, seismic simulations were carried out by using explosive source (Virieux, 1986; and Olsen et al., 1995). The explosive source simulation is not physically realisable since it cannot explain the observed radiation patterns and is dominated by compressional waves. The successful numerical implementation of double-couple point source was presented by Vidale et al. (1987), Frankel and Vidale (1992), Coutant et al. (1995), Graves (1996), Pitarka (1999) and Narayan (2001). Although Vidale et al. (1987) used the Alterman and Karal (1968) procedure to generate double-couple source, they have not paid any attention to numerical source description. The source implementation based on moment tensor formulation is relatively simpler and contains the complete source description (Aki and Richards, 1980; and Pitarka, 1999).

3-D elastodynamic wave equations were approximated using the parsimonious staggered grid approximation (Ohminato and Chouet, 1997) and corresponding algorithm was developed. The double couple point shear dislocation source with a particular focal mechanism based on moment tensor formulation (Aki and Richards, 1980; and Pitarka, 1999) was implemented into the numerical grid. The radial, transverse and vertical components of the radiation pattern for different focal mechanisms were computed. The different components of the ground displacement were computed using moment per unit volume for comparative study, by varying the grid size of the finite difference cell. Vacuum formulation was used at the free surface for stability. Sponge boundary condition was implemented on the model edges to avoid edge reflections (Israeli and Orszag, 1981). The effects of soil velocity were studied since they play an important role in the amplitude amplification, changes in signal duration, frequency content and mode conversion.

NUMERICAL APPROXIMATION OF 3-D WAVE EQUATION

3-D elastodynamic wave equations for a linear, isotropic elastic media without source are as follows

$$\begin{aligned}\rho\partial_t u &= \partial_x\sigma_{xx} + \partial_y\sigma_{xy} + \partial_z\sigma_{xz}\\ \rho\partial_t v &= \partial_x\sigma_{xy} + \partial_y\sigma_{yy} + \partial_z\sigma_{yz}\\ \rho\partial_t w &= \partial_x\sigma_{xz} + \partial_y\sigma_{yz} + \partial_z\sigma_{zz}\end{aligned} \tag{1}$$

and stress-strain relations are

$$\begin{aligned}\sigma_{xx} &= (\lambda+2\mu)\partial_x u + \lambda(\partial_y v + \partial_z w)\\ \sigma_{yy} &= (\lambda+2\mu)\partial_y v + \lambda(\partial_x u + \partial_z w)\\ \sigma_{zz} &= (\lambda+2\mu)\partial_z w + \lambda(\partial_x u + \partial_y v)\\ \sigma_{xy} &= \mu(\partial_y u + \partial_x v)\\ \sigma_{xz} &= \mu(\partial_z u + \partial_x w)\\ \sigma_{yz} &= \mu(\partial_z v + \partial_y w)\end{aligned} \tag{2}$$

Here, $(u, v \text{ and } w)$ are the displacement components; $(\sigma_{xx}, \sigma_{yy}, \sigma_{zz}, \sigma_{xz}, \sigma_{xy}$ and $\sigma_{yz})$ are the stress components; ρ is density; λ and μ are the Lame's coefficients; and the symbols ∂_x, ∂_y, ∂_z *and* ∂_t are shorthand representations of the differential operators ∂/∂_x, ∂/∂_y, ∂/∂_z and $\partial^2/\partial t^2$, respectively.

3-D elastodynamic wave equation was approximated using parsimonious staggered grid scheme (Ohminato and Chouet, 1997). This scheme requires only about 75% of the computational memory as required by the standard staggered grid scheme (Virieux, 1986). Further, it is stable for full range of Poisson's ratio and is free from the spatial derivative of elastic parameters. The parsimonious scheme based on the displacement-stress relation is best suitable for the computation of dislocation as compared to velocity-stress relation (Coutant et al., 1995).

The time and spatial derivatives of Equations (1) and (2) were replaced by the second order parsimonious staggered grid differencing operator as follows:

$$\begin{aligned}\rho_{l,m,n}\left[\frac{u^{t+1}_{l,m,n}+u^{t-1}_{l,m,n}-2u^{t}_{l,m,n}}{\Delta t^2}\right] &= \left[\frac{(\sigma_{xx})^{t}_{l,m,n}-(\sigma_{xx})^{t}_{l-1,m,n}}{\Delta x}\right]+\left[\frac{(\sigma_{xy})^{t}_{l,m+1,n}-(\sigma_{xy})^{t}_{l,m,n}}{\Delta y}\right]\\ &+\left[\frac{(\sigma_{xz})^{t}_{l,m,n+1}-(\sigma_{xz})^{t}_{l,m,n}}{\Delta z}\right]\\ \rho_{l,m,n}\left[\frac{v^{t+1}_{l,m,n}+v^{t-1}_{l,m,n}-2v^{t}_{l,m,n}}{\Delta t^2}\right] &= \left[\frac{(\sigma_{xy})^{t}_{l+1,m,n}-(\sigma_{xy})^{t}_{l,m,n}}{\Delta x}\right]+\left[\frac{(\sigma_{yy})^{t}_{l,m,n}-(\sigma_{yy})^{t}_{l,m-1,n}}{\Delta y}\right]\\ &+\left[\frac{(\sigma_{xy})^{t}_{l,m,n+1}-(\sigma_{xy})^{t}_{l,m,n}}{\Delta z}\right]\end{aligned} \tag{3}$$

$$\rho_{l,m,n}\left[\frac{w^{t+1}_{l,m,n}+w^{t-1}_{l,m,n}-2w^{t}_{l,m,n}}{\Delta t^2}\right]=\left[\frac{(\sigma_{xx})^{t}_{l+1,m,n}-(\sigma_{xx})^{t}_{l,m,n}}{\Delta x}\right]+\left[\frac{(\sigma_{xy})^{t}_{l,m+1,n}-(\sigma_{xy})^{t}_{l,m,n}}{\Delta y}\right]+\left[\frac{(\sigma_{xz})^{t}_{l,m,n}-(\sigma_{xz})^{t}_{l,m,n-1}}{\Delta z}\right]$$

The stress-strain relations are given by

$$(\sigma_{xx})^{t}_{l,m,n}=(\lambda_{l,m,n}+2\mu_{l,m,n})\left(\frac{u^{t}_{l+1,m,n}-u^{t}_{l,m,n}}{\Delta x}\right)+\lambda_{l,m,n}\left(\frac{v^{t}_{l,m+1,n}-v^{t}_{l,m,n}}{\Delta y}+\frac{w^{t}_{l,m,n+1}-w^{t}_{l,m,n}}{\Delta z}\right)$$

$$(\sigma_{yy})^{t}_{l,m,n}=(\lambda_{l,m,n}+2\mu_{l,m,n})\left(\frac{v^{t}_{l,m+1,n}-v^{t}_{l,m,n}}{\Delta y}\right)+\lambda_{l,m,n}\left(\frac{u^{t}_{l+1,m,n}-u^{t}_{l,m,n}}{\Delta x}+\frac{w^{t}_{l,m,n+1}-w^{t}_{l,m,n}}{\Delta z}\right)$$

$$(\sigma_{zz})^{t}_{l,m,n}=(\lambda_{l,m,n}+2\mu_{l,m,n})\left(\frac{w^{t}_{l,m,n+1}-w^{t}_{l,m,n}}{\Delta z}\right)+\lambda_{l,m,n}\left(\frac{u^{t}_{l+1,m,n}-u^{t}_{l,m,n}}{\Delta x}+\frac{v^{t}_{l,m+1,n}-v^{t}_{l,m,n}}{\Delta y}\right)$$

$$(\sigma_{xy})^{t}_{l,m,n}=\mu_{l,m,n}\left(\frac{v^{t}_{l,m,n}-v^{t}_{l-1,m,n}}{\Delta x}+\frac{u^{t}_{l,m,n}-u^{t}_{l,m-1,n}}{\Delta y}\right) \quad (4)$$

$$(\sigma_{xz})^{t}_{l,m,n}=\mu_{l,m,n}\left(\frac{u^{t}_{l,m,n}-u^{t}_{l,m,n-1}}{\Delta z}+\frac{w^{t}_{l,m,n}-w^{t}_{l-1,m,n}}{\Delta x}\right)$$

$$(\sigma_{zy})^{t}_{l,m,n}=\mu_{l,m,n}\left(\frac{v^{t}_{l,m,n}-v^{t}_{l,m,n-1}}{\Delta z}+\frac{w^{t}_{l,m,n}-w^{t}_{l,m-1,n}}{\Delta y}\right)$$

The use of stresses at time t in Equation (3), which were computed using differenced stress-strain relations (Equation (4)), is the main reason of the parsimony. Here, Δt is the time step and $\Delta x = \Delta y = \Delta z$ are the grid intervals in the x-, y- and z-direction, respectively. l, m and n are the grid indices in the x-, y- and z-directions, and t is the time index.

FREE SURFACE AND ABSORBING BOUNDARY

Free surface boundary conditions often require careful consideration in numerical schemes for stability and accuracy. In the present study, vacuum formulation was adopted in which α, β and $\rho \to 0$ in the region above the free surface (Graves, 1996). Graves (1996) reported that this formulation is stable for second order schemes and unstable for fourth order schemes. Therefore, there is no stability problem in the incorporation of vacuum formulation at the free surface since a used parsimonious scheme is second order accurate. The vacuum formulation is useful in modelling the effects of surface topography. It can be implemented with the same difference equation as used in the interior of the model. A sponge boundary condition developed by Israeli and Orszag (1981) was implemented on the model edges to avoid the edge reflections.

MOMENT TENSOR SOURCE IMPLEMENTATION

The double-couple point source was implemented into the computational grid, based on the moment tensor source formulation that uses stress tensor components at the source location (Pitarka, 1999). The equivalent body forces were added to each component of the stress tensor at every time step in contrast to body forces to each velocity components as used by Graves (1996). 3-D stress tensor components for a source location at the grid point, (l, m, n) are given below:

$$
\begin{aligned}
(\sigma_{xx})^{n}_{l,m,n} &= (\sigma_{xx})^{n}_{l,m,n} - \frac{M_{xx}(t)}{V} \\
(\sigma_{yy})^{n}_{l,m,n} &= (\sigma_{yy})^{n}_{l,m,n} - \frac{M_{yy}(t)}{V} \\
(\sigma_{zz})^{n}_{l,m,n} &= (\sigma_{zz})^{n}_{l,m,n} - \frac{M_{zz}(t)}{V} \\
(\sigma_{xz})^{n}_{l,m,n} &= (\sigma_{xz})^{n}_{l,m,n} - \frac{M_{xz}(t)}{V} \\
(\sigma_{xy})^{n}_{l,m,n} &= (\sigma_{xy})^{n}_{l,m,n} - \frac{M_{xy}(t)}{V} \\
(\sigma_{zy})^{n}_{l,m,n} &= (\sigma_{zy})^{n}_{l,m,n} - \frac{M_{zy}(t)}{V}
\end{aligned}
\tag{5}
$$

Here, $M_{xx}(t)$, $M_{yy}(t)$, $M_{zz}(t)$, $M_{xy}(t)$, $M_{xz}(t)$, and $M_{zy}(t)$ are the moment tensor components (Aki and Richards, 1980). V is the volume of the finite difference cell instead of the volume of the material cell since the effective finite difference grid size is half of the material grid size (Ohminato and Chouet, 1997).

A simple homogeneous model was simulated using different amount of moment. Moment was varied in the simulation by varying the finite difference grid size (cell volume) for a fixed value of moment per unit volume. The second derivative of convolution of a polynomial window, $\left\{1-(\tau-1)^2\right\}^{\beta}$ and the Gaussian function, $\exp\left\{-\alpha(T-T_0)^2\right\}$ with a dominant period T_0 was used as a source function, where τ is equal to T/T_0. The model parameters, namely Lame's parameters (λ and μ), density and dominant frequency were taken as 10.0 GPa, 10.0 GPa, 2.5 g/cc and 1.5 Hz, respectively. Radial, transverse and vertical components of the ground displacement were computed at an offset of 6.3 km by using a double couple point source with a focal mechanism of strike = 90°, dip = 45° and rake = 90° and at a depth of 6.5 km.

The different moment tensor components in the form of stresses have been applied on the different faces of a cubical grid for generating the point shear dislocation source. Thus, the volume of that cube will decide the volume in which moment has been released, although moment per unit volume is a fixed quantity. Therefore, total moment released will depend on the volume of the cubical numerical grid. Simulations were carried out using different grid size (90 m, 100 m, and 110 m) to verify the effect of variation of volume of cubical grid on the ground motion for a fixed amount of moment per unit volume (Table 1). In this way, the total moment used in each case was different depending on the effective volume of the finite difference cell. Figure 1 shows radial, transverse and vertical components of the amplitude responses for different grid sizes. Results reveal that the variation in ground displacement is in agreement with the total moment used (volume of cubical grid multiplied with moment per unit volume). The variations of the maximum ground displacements in radial, transverse and vertical components for different grid sizes are noted in Table 1.

Table 1: Maximum Ground Displacement Caused by a Source with a Focal Mechanism of Strike = 90°, Dip = 45°, and Rake = 90° over a Half-Space

Material Grid Size Δx (m)	Moment per Unit Volume (N/m^2)	GROUND DISPLACEMENT (cm)					
		Radial component		Transverse component		Vertical component	
		Max (-)	Max (+)	Max (-)	Max (+)	Max (-)	Max (+)
90	10^{11}	7.19	10.92	2.73×10^{-2}	2.72×10^{-2}	39.38	53.21
100	10^{11}	13.30	14.77	2.61×10^{-2}	1.51×10^{-2}	52.07	71.72
110	10^{11}	19.37	20.44	1.93×10^{-2}	1.54×10^{-2}	64.42	90.28

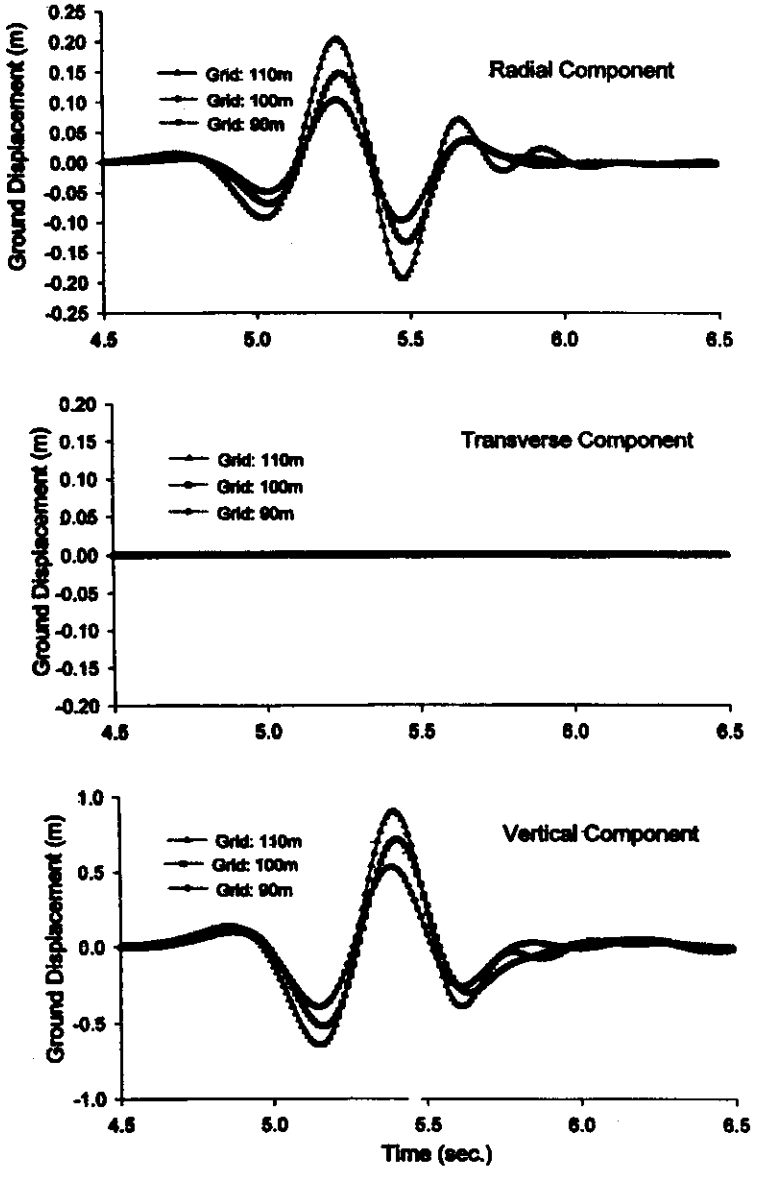

Fig. 1 Radial, transverse and vertical responses of a half-space model using different grid size

3-D RADIATION PATTERN

The radiation patterns for different source mechanisms were computed in the form of snapshots using moment tensor components in a Cartesian coordinate system (Aki and Richards, 1980). Snapshots (ground displacement on each grid point at a particular moment) were computed for different components of the radiation pattern for a homogeneous model with equal Lame's parameters and density as 10.0 GPa and 2.5 g/cc, respectively. The length, width and height of the model were 15.0 km, 15.0 km and 3.0 km, respectively, and source was kept in the center at a depth of 1.0 km. The snapshots were computed after 2.5 s. Modelling parameters, grid size, time step and dominant frequency, were 100.0 m, 0.01 s and 2.0 Hz, respectively. Figures 2(a), 2(b) and 2(c) show the radial, transverse and vertical components of radiation pattern on the surface using a double couple point shear dislocation source with focal mechanism of strike = 45^0, dip = 90^0 and rake = 0.0^0. There are four shear and compressional lobes in all the components of radiation pattern. It should be noted that the shear component is more dominating in the vertical component as compared to two horizontal components in this particular case. Maximum

positive amplitude in the snapshots is shown by black colour, and negative amplitude is shown by white colour through out the paper.

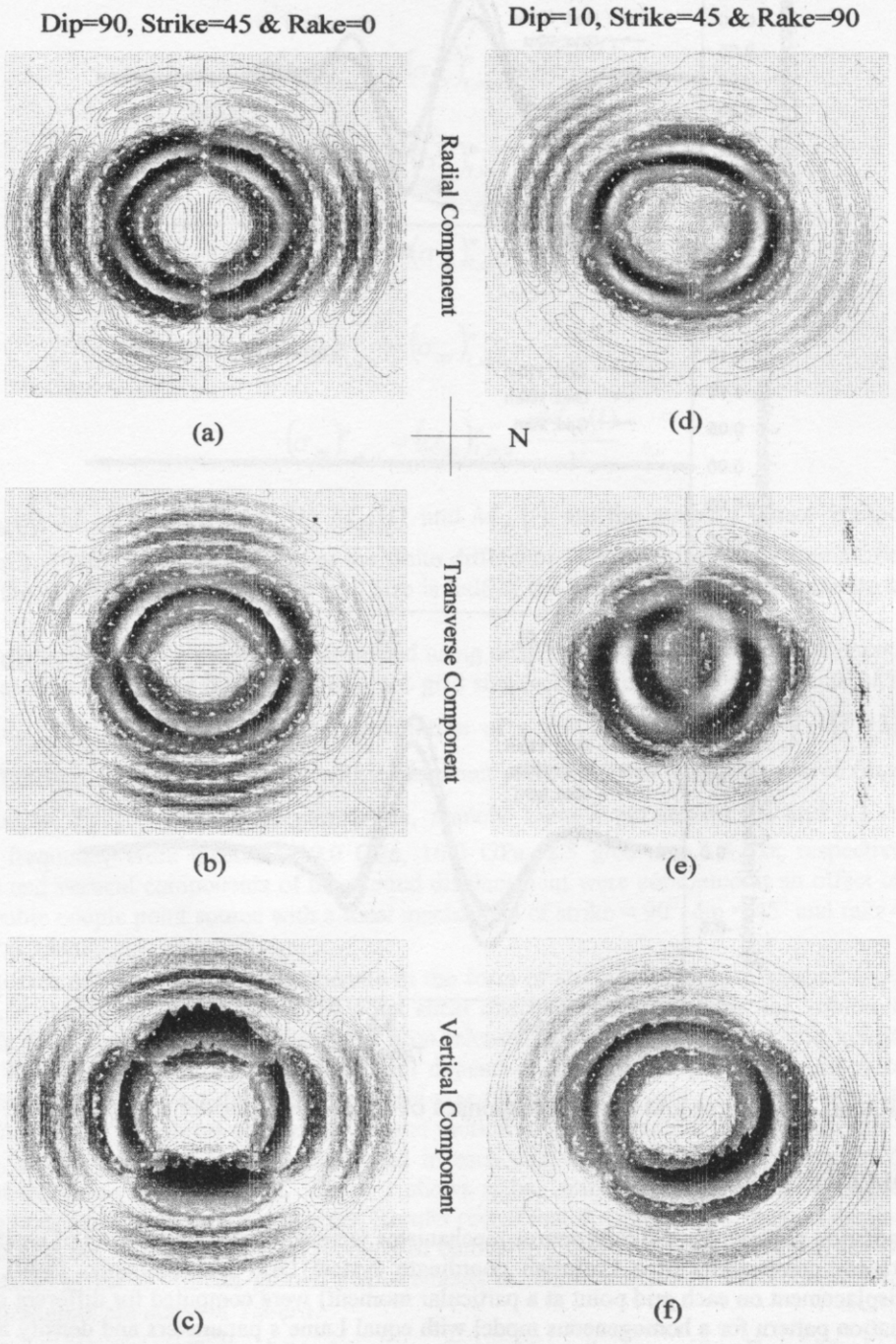

Fig. 2 Radial, transverse and vertical components of radiation pattern using double-couple point sources with different focal mechanism

Similarly, Figures 2(d), 2(e) and 2(f) respectively show the radial, transverse and vertical components of radiation pattern using a source with focal mechanism of strike = 45^0, dip = 10^0 and rake = 90^0. In this case, there are four shear and compressional lobes in both the horizontal components, but there are only two shear and compressional lobes in the vertical component. Shear component is dominating in the vertical component and will be more damaging in the strike direction. The elongation of damage in the

strike direction (which may be due to the effect of source finiteness in case of moderate to large earthquakes) was also reported by Kaila and Sarkar (1978), based on the analysis of the isoseismals of the major Indian earthquakes.

APPLICATION OF ATTENUATION FUNCTION

An approximate technique for modelling of spatially varying visco-elastic media using time domain attenuation operator (Graves, 1996) was used in the present study. In the frequency domain, anelastic attenuation operators are well understood and easy to implement using the quality factor Q (Aki and Richards, 1980). In the broad-band simulations, frequency-dependent attenuation coefficient and wave velocity are required to produce an accurate result. But the implementation of frequency-dependent attenuation operator and wave velocity in the time domain is difficult and requires large computational time and storage (Carcione et al., 1988). However, for limited bandwidth, an appropriate reference frequency in the middle of the desired band can be used. In the present simulation, a wavelet with dominant frequency, f_0, almost in the center of the frequency band is used as a reference frequency to avoid the above-mentioned problems. In the computations, all frequencies will be attenuated by the same amount. It means that higher frequencies will be under-attenuated and lower frequencies will be over-attenuated. However, it seems reasonably acceptable since limited frequency band is used in the simulation. In addition, since the variations in phase velocity are typically less than 1% to 2% for the period range, 1-20 seconds, the reference velocity corresponding to f_0 can be used as a good approximation to the variation of phase velocity in the used frequency band (Graves, 1996). The attenuation function (A), depending on only reference frequency f_0 is given below :

$$A = \exp\left(\frac{-\pi f_0 t}{Q}\right) \tag{6}$$

The attenuation function is applied to both the updated displacement and stress fields after each time step (Δt), since both fields have propagated during each time update. Quality factor can vary from grid to grid, depending on the complexity of the media. The modified attenuation function at a point, (l, m, n) for time duration Δt is given below :

$$A_{l,m,n} = \exp\left(\frac{-\pi f_0 \Delta t}{Q^s_{l,m,n}}\right) \tag{7}$$

Q^s (quality factor for shear wave) is used in the attenuation function since earthquake motions are dominated by shear wave and it is difficult to distinguish between the P- and S-waves in the finite difference calculations. P-waves will be over-attenuated in the modelling, since Q^p is usually larger than Q^s.

A homogeneous model was simulated with and without attenuation at two epicentral distances, using a double-couple point source with focal mechanism of dip = 10.0^0, rake = 90.0^0 and strike = 45.0^0. The model size was 10x6x80 km, and source was generated at 5.8 km depth. The model parameters, namely Lame's parameters $(\lambda$ and $\mu)$, density, constant quality factor (Q), dominant frequency, grid size and sampling period were taken as 10.0 GPa, 10.0 GPa, 2.5 g/cc, 60.0, 2.2 Hz, 100.0 m and 0.01 s, respectively. Figures 3(a) and 3(b) show the responses with and without attenuation in time domain and frequency domain respectively at the epicenter. The response in frequency domain depicts that effects of attenuation are maximum for dominant frequency and these are decreasing in both higher and lower frequency sides, but the effects should be high for high frequency. This is the main drawback of incorporating the attenuation in the time domain but practically it is reasonable since earthquake engineers are interested in a limited frequency band. Similarly, Figures 3(c) and 3(d) show the response at an offset of 3.0 km with a similar effect of attenuation.

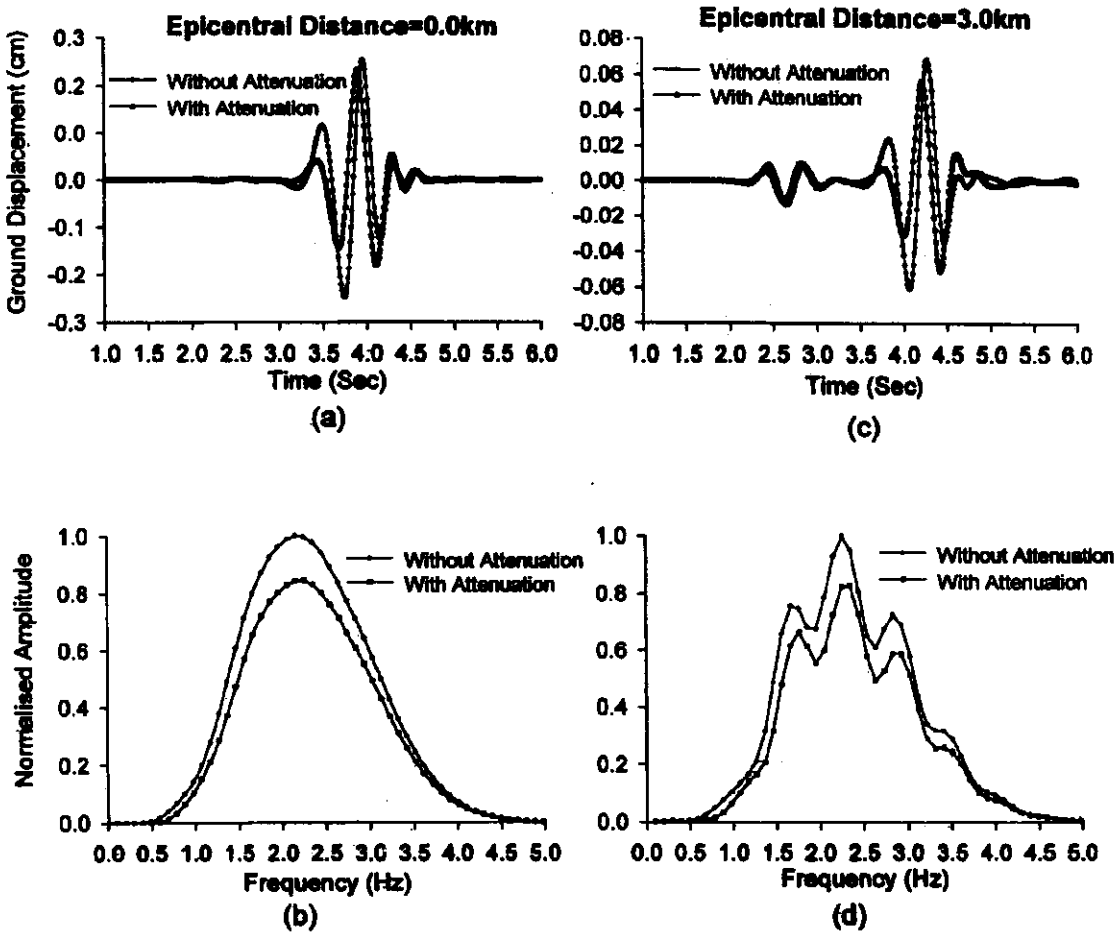

Fig. 3 Effect of attenuation on the radial responses of a half-space model

Table 2: Parameters and the Layer Thickness of a Geological Model

Layer	Thickness	Depth	V_p (m/s)	V_s (m/s)	μ (GPa)	λ (GPa)	Density g/cc
1.	1.00 km	1.00 km	1700.0	1000.0	02.000	01.780	2.00
2.	1.00 km	2.00 km	2301.0	1342.8	04.508	04.232	2.50
3.	2.00 km	4.00 km	3464.1	2000.0	10.000	10.000	2.50
4.	2.00 km	6.00 km	4300.7	2500.4	15.630	14.980	2.50
5.	-	-	6097.9	3531.4	35.630	34.980	2.85

AMPLITUDE BEHAVIOUR IN A LAYERED MEDIA

Snapshots of a five layered geological model (Figure 4) were computed in the x-z plane using a double couple point shear dislocation source with focal mechanism of dip = 45.0^0, rake = 90.0^0 and strike = 0.0^0, to study the behaviour of wavefront at different discontinuities encountered in the path and to examine the accuracy of the parsimonious staggered grid scheme. The meaning of snapshot is to register the ground displacement on each grid point at a particular moment. The model dimension is shown in Figure 4, and model parameters are listed in Table 2. The grid size, time step, focal depth and dominant frequency were taken as 100.0 m, 0.005 s, 8.0 km and 1.0 Hz, respectively. The moment per unit volume used in the simulation was 10^{11} N/m^2. Figure 5 shows snapshots of radial component at 2.0 s, 3.0 s, 4.0 s, 5.0 s, 6.0 s, 7.0 s, 8.0 s and 9.0 s. Snapshot at time 2.0 s shows three shear and compressional lobes. Tremendous amplitude amplification is visible in the surficial layer at time 6.0 s. The upgoing

primary S-phase and the reflected Pp-phase from the surface are clearly visible at 4.0, 5.0 and 6.0 s. Reflected Pp- and Ss-phases from the surface are also clearly visible in the snapshots at times 7.0 s and 8.0 s. Similarly, snapshots at times 8.0 s and 9.0 s depict the reflected Pp- and Ss-phases, multiples and the new phases in the surficial layer. The decrease and increase of the wavelength in different layers depending on the velocity of the layer can be easily inferred from snapshots.

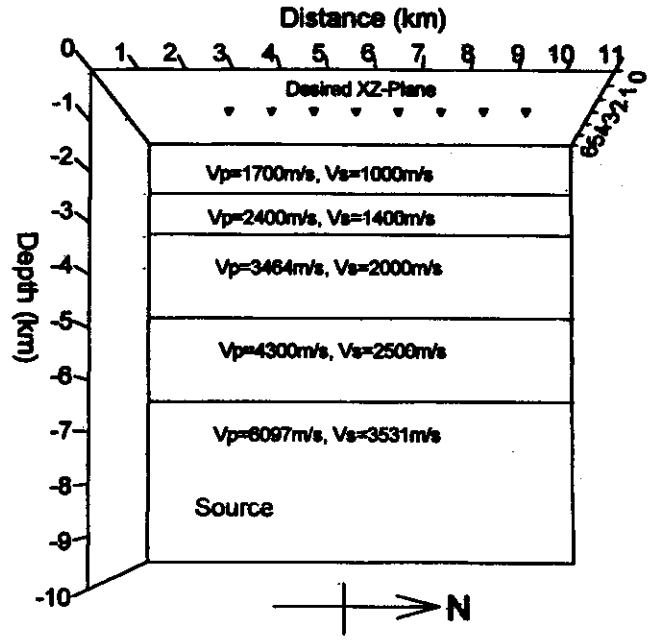

Fig. 4 Five-layered geological model

Figures 6(a) and 6(b) show the maximum negative and positive amplitude present in the snapshots of radial component at various times. There is a fast decrease of amplitude in the wavefronts upto 3.0 s, and then amplification starts as the wave enters the second layer. Increase of the amplitude in the wave front is due to the amplitude amplification caused by decrease of shear strength in the overlying layers. Amplitude amplification at time 6.0 s is due to the amplification caused by sudden decrease of shear strength in the surficial layer as well as due to possible interference of the outgoing wavefront and the reflected wavefront.

EFFECT OF SOIL VELOCITY

Four three-layer models (Table 3) with different velocities in the surficial layer were simulated to study the effects of soil velocity and resonance on the characteristics of the ground motion. The material properties are common for the Layer 2 and Layer 3 in all the four models. The velocity and density of the surficial layer (Layer 1) of Model M1 are taken same as those of Layer 2 for the purpose of comparison and to compute the spectral ratio for Models M2-M4 with respect to Model M1. The grid size, time step, dominant frequency and model size were taken as 50.0 m, 0.005 s, 2.2 Hz and 8x6x10 km, respectively. Various parameters of the example models are listed in Table 3. Figure 7(a) shows the radial component of the ground displacement at zero offset (epicenter) caused by a point source with focal mechanism of dip = 10.0^0, rake = 90.0^0 and strike = 45.0^0 at a depth of 8.0 km, for the different models. The maximum ground displacement is shown at the right end of each trace. The comparison of these responses depicts that shear wave is dominating in the radial component at the epicenter and both the ground displacement and duration are increasing with the decrease of velocity in the surficial layer. The corresponding amplitude spectra shown in Figure 7(b) depict the similar effect in amplitude amplification. Spectral ratios were computed to find out the amplitude amplification factor for Models M2, M3, and M4 with respect to Model M1. Figure 7(c) depicts the spectral ratios of Models M2, M3, and M4. Average amplifications in radial component for Models M2, M3, and M4 are 1.17, 1.89 and 3.79, respectively.

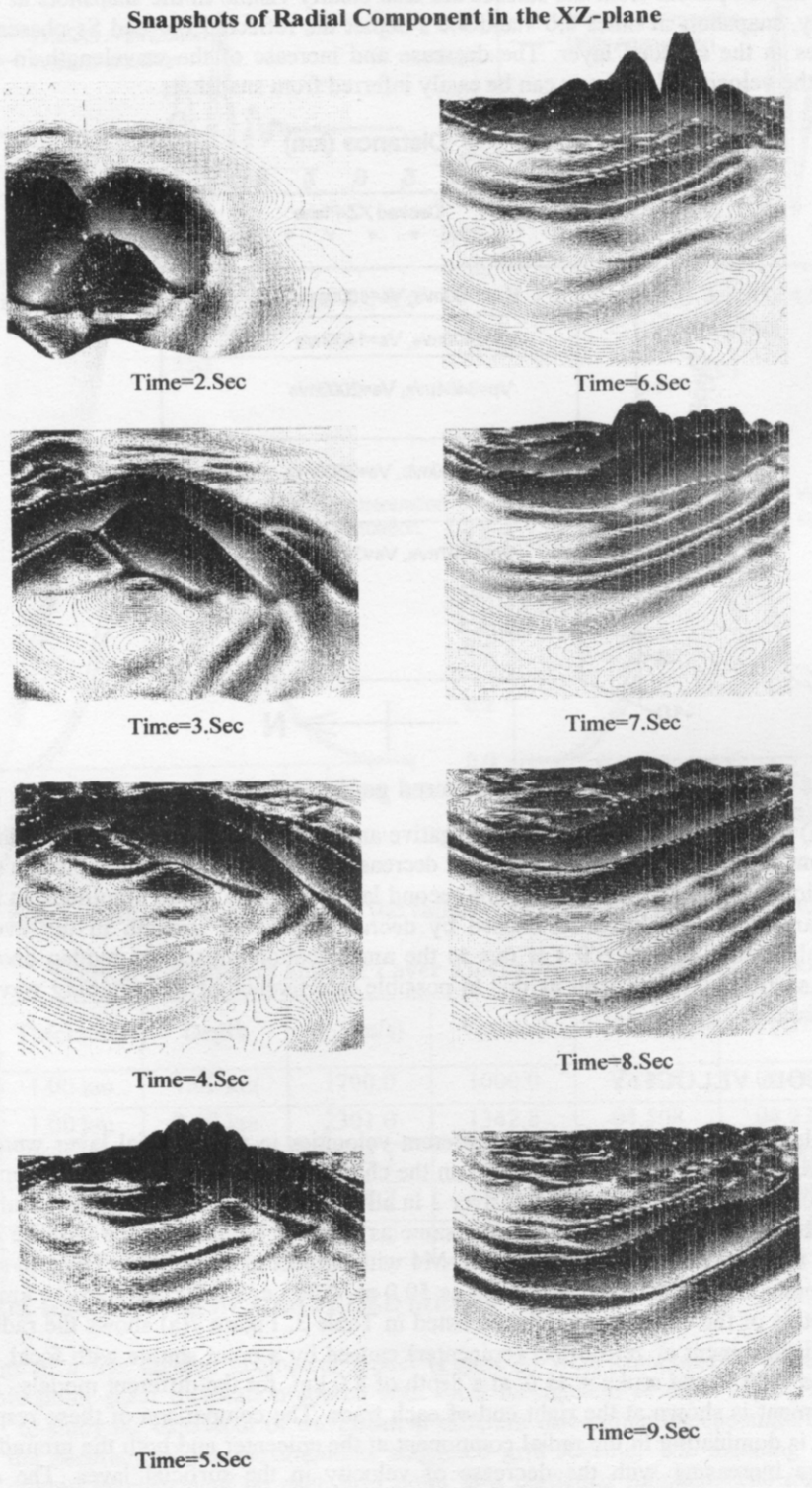

Fig. 5 Snapshots (radial component) at different times of model (Fig. 4) using point source with focal mechanism of dip = 90.0^0, rake = 0.0^0 and strike = 0.0^0

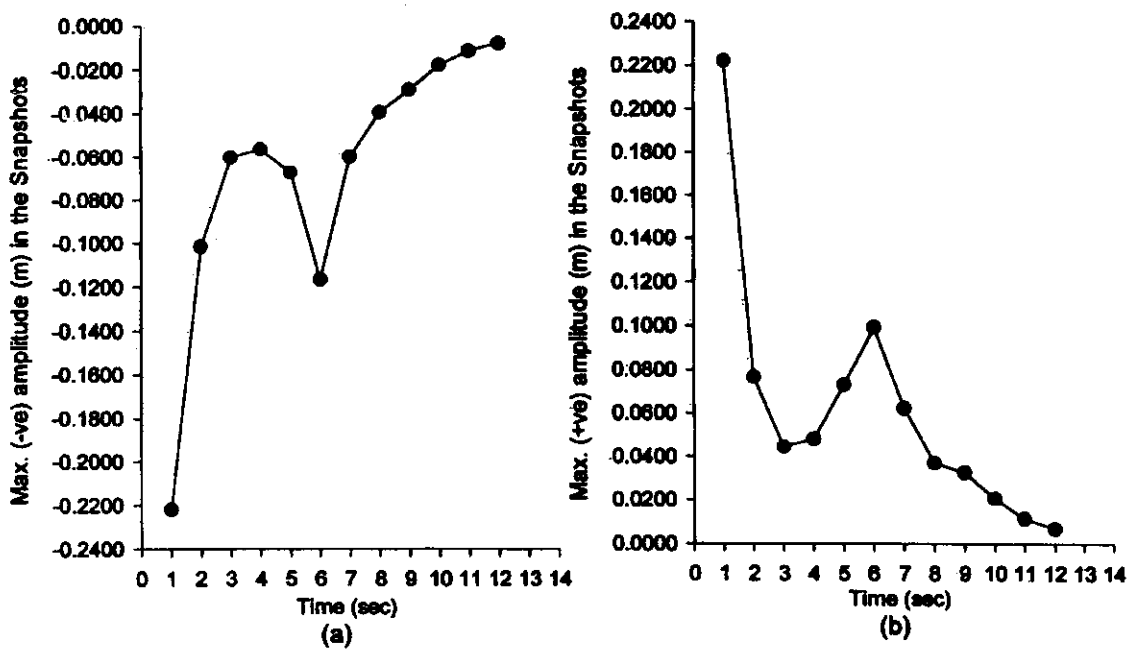

Fig. 6 Amplitude variation of propagating wavefront in a layered media

Table 3: Parameters and Thickness of Different Geological Models

Layer	Thickness	Parameters	Model 'M1'	Model 'M2'	Model 'M3'	Model 'M4'
1.	0.50 km	V_p (m/s)	3826.23	3464.10	3000.00	2200.00
		V_s (m/s)	2209.07	2000.00	1500.00	1000.00
		ρ (g/cc)	2.50	2.50	2.40	2.20
2.	1.00 km	V_p (m/s)	3826.23	3826.23	3826.23	3826.23
		V_s (m/s)	2209.07	2209.07	2209.07	2209.07
		ρ (g/cc)	2.50	2.50	2.50	2.50
3.	-	V_p (m/s)	4167.33	4167.33	4167.33	4167.33
		V_s (m/s)	2406.01	2406.01	2406.01	2406.01
		ρ (g/cc)	2.70	2.70	2.70	2.70

Similar effects in increase of signal duration and amplitude amplification can be observed in the transverse component as shown in Figure 7(d). Average amplifications in transverse component (Figure 7(f)) for Models M2, M3, and M4 are 1.18, 1.93 and 3.76, respectively. Figure 7(g) depicts the vertical responses in time domain for different models. The ground displacement caused by compressional wave is of same order as that by the shear wave. The average amplitude amplifications in vertical component for Models M2, M3, and M4 are 1.08, 1.34 and 1.99 respectively, which are much lesser than those in the two horizontal components. There is even a de-amplification for some frequencies.

DISCUSSION AND CONCLUSIONS

An algorithm for 3-D modelling was developed using parsimonious staggered grid scheme (Ohminato and Chouet, 1997). It was adopted instead of standard staggered grid scheme (Virieux, 1996) since it requires lesser computational memory (only 75%) and enjoys the same advantage of being stable for larger Poisson's ratio and free from spatial derivative of elastic parameters. In the present study, vacuum formulation was adopted in which α, β and $\rho \rightarrow 0$ in the region above the free surface (since it is

useful in simulating the effects of surface topography (Graves, 1996)). Double-couple point dislocation source was implemented into the computational grid, based on the moment tensor source formulation that uses stress tensor components at the source location (Pitarka, 1999).

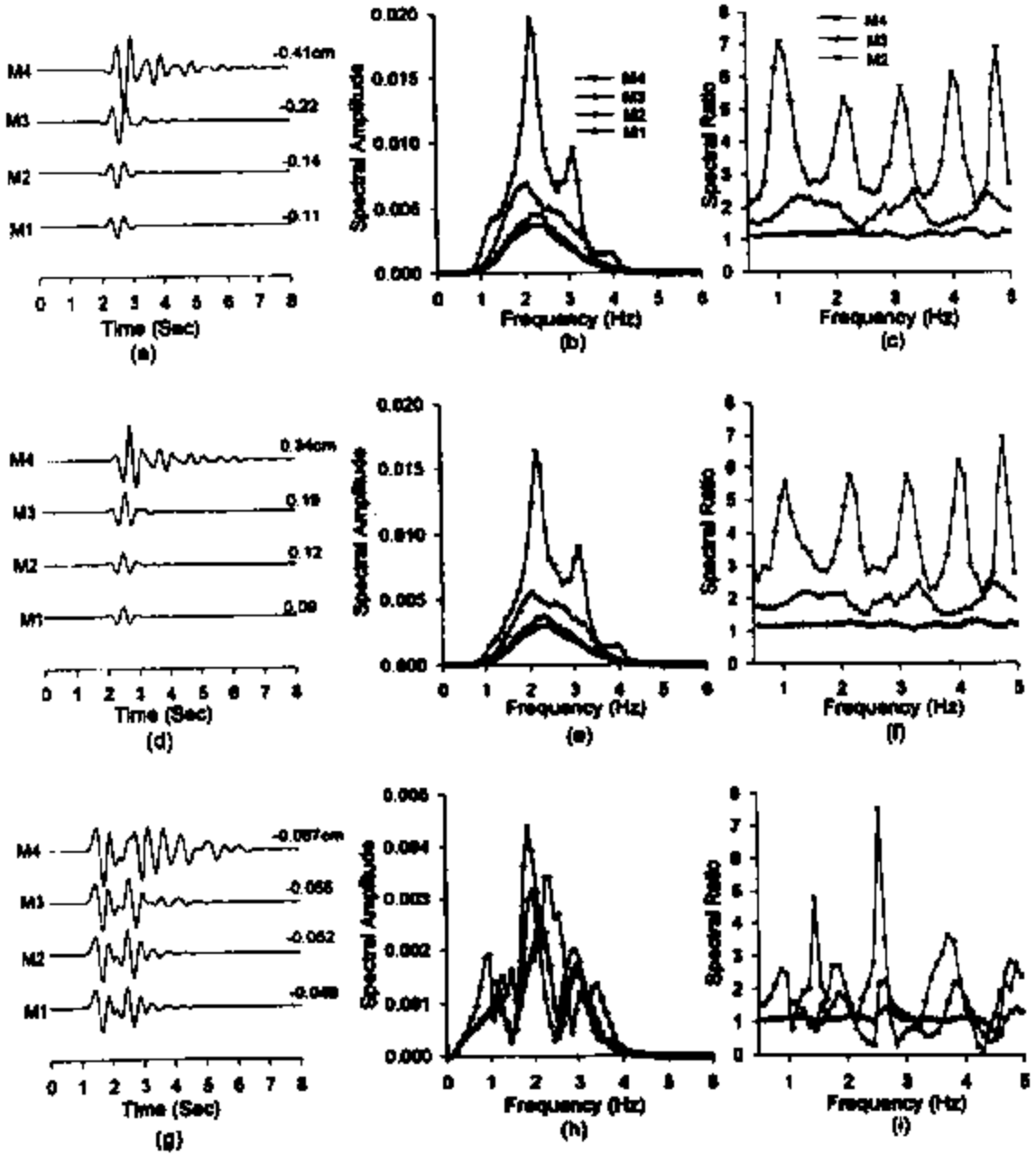

Fig. 7 Effects of soil velocity in the surficial layer on the ground motion characteristics

Simulated results for a half-space model with different grid sizes using a fixed amount of moment per unit volume are in accordance with the effectively used moment in the source generation. The amplitude behaviour and generation of different seismic phases at discontinuities encountered in the path prove the accuracy and stability of the parsimonious staggered grid scheme as well as the vacuum formulation at the free surface. Anelastic attenuation was incorporated in the modelling by applying a simple attenuation function to both updated displacement and stress fields after each time step, and the result is fulfilling the aim for a desired frequency band (Graves, 1996). The incorporation of anelastic attenuation in the numerical simulation is very important, particularly when studying the effects of various types of soils on the ground motion characteristics, since waves attenuate at faster rates in soils as compared to hard rocks.

The effect of soil velocity on the amplitude amplification and duration was studied and results depict that there is an increase in amplification and duration with decrease of velocity in the surficial layer. Further, it was found that horizontal components were more amplified compared to the vertical components, based on spectral ratio method. The development of 3-D modelling for site-specific ground motion prediction taking into account the energy released, radiation pattern, path effect and local site conditions will be very useful for earthquake resistant design, seismic microzonation, and damage and loss scenario in the area, when there is no ground motion record.

ACKNOWLEDGMENTS

Financial assistance by Indian National Science Academy (INSA), New Delhi is gratefully acknowledged.

REFERENCES

1. Aki, K. and Richards, P.G. (1980). "Quantitative Seismology", W.H. Freeman and Co., San Francisco, U.S.A.
2. Alterman, Z.S. and Keral, Jr., F.C. (1968). "Propagation of Elastic Waves in Layered Media by Finite Difference Methods", Bull. Seism. Soc. Am., Vol. 58, pp. 367-398.
3. Anderson, J.G., Bodin, P., Brune, N.J., Prince, J., Singh, S.K., Quaas, R. and Onate, M. (1986). "Strong Ground Motion from the Michoacan, Mexico Earthquake", Science, Vol. 233, pp. 1043-1049.
4. Boore, D.M. and Joyner, W.B. (1997). "Site Amplification of Generic Rock Sites", Bull. Seism. Soc. Am., Vol. 87, pp. 327-341.
5. Carcione, J.P., Kosloff, D. and Kosloff, R. (1988). "Wave Propagation Simulation in a Linear Viscoelastic Media", Geophysical Journal International, Vol. 95, pp. 597-611.
6. Coutant, O., Virieux, J. and Zollo, A. (1995). "Numerical Source Implementation in a 2-D Finite Difference Scheme for Wave Propagation", Bull. Seism. Soc. Am., Vol. 85, pp. 1507-1512.
7. Frankel, A. and Vidale, J. (1992). "A Three-Dimensional Simulation of Seismic Waves in the Santa Clara Valley, California, from a Loma Prieta Aftershock", Bull. Seism. Soc. Am., Vol. 82, pp. 2045-2074.
8. Graves, R.W. (1996). "Simulating Seismic Wave Propagation in 3-D Elastic Media using Staggered Grid Finite Difference", Bull. Seism. Soc. Am., Vol. 86, pp. 1091-1106.
9. Israeli, M. and Orszag, S.A. (1981). "Approximation of Radiation Boundary Conditions", J. Comp. Phys., Vol. 41, pp. 115-135.
10. Kaila, K.L. and Sarkar, D. (1978). "Atlas of Isoseismal Maps of Major Earthquakes in India", Geophys. Res. Bulletin, Vol. 16, pp. 233-267.
11. Mikumo, T. and Miyatake, T. (1987). "Numerical Modelling of Realistic Fault Rupture Process", in Seismic Strong Motion Synthetics (Bolt, B.A., ed.), Academic Press, Orlando, Florida, U.S.A.
12. Narayan, J.P. (2000). "Strong Ground Motion Simulation Using Shear Dislocation Sources", Geophyzika, Vol. 16-17, pp. 73-86.
13. Narayan, J.P. (2001). "Site Specific SGM Prediction Using 2.5-D Modelling", Geophysical Journal International, Vol. 146, pp. 269-281.
14. Ohminato, T. and Chouet, B.A. (1997). "A Free Surface Boundary Condition for including 3-D Topography in the Finite Difference Method", Bull. Seism. Soc. Am., Vol. 87, pp. 494-515.
15. Olsen, K.B., James, C.P. and Schuster, G.T. (1995). "Simulation of 3-D Elastic Wave Propagation in the Salt Lake Basin", Bull. Seism. Soc. Am., Vol. 85, pp. 1688-1710.
16. Pitarka, A. (1999). "3-D Elastic Finite Difference Modelling of Seismic Motion Using Staggered Grids with Nonuniform Spacing", Bull. Seism. Soc. Am., Vol. 89, pp. 54-68.
17. Vidale, J.E. and Helmberger, D.V. (1987). "Path Effect in Strong Motion Seismology", in Seismic Strong Motion Synthetics (Bolt, B.A., ed.), Academic Press, Orlando, Florida, U.S.A.
18. Virieux, J. (1986). "P-SV Wave Propagation in Heterogeneous Media, Velocity Stress Finite-Definite Method", Geophysics, Vol. 51, pp. 889-901.